Monte Carlo Simulation Studies on the Structure of the Counterion Atmosphere of B-DNA. Variations on the Primitive Dielectric Model

B. Jayaram, S. Swaminathan, and D. L. Beveridge*

Department of Chemistry, Wesleyan University, Middletown, Connecticut 06457

K. Sharp and B. Honig

Department of Biochemistry and Molecular Biophysics, Columbia University, New York, New York 10032

Received October 2, 1989; Revised Manuscript Received December 27, 1989

ABSTRACT: Monte Carlo computer experiments on the structure and organization of counterions around a B form of a DNA double helix in aqueous media have been carried out, treating water in the system as a modified homogeneous dielectric. The detailed shape of the DNA and, the finite size and spatial correlations of the counterions are taken into account. Convergence criteria, step size, single-particle versus multiparticle moves, and other methodological issues in the Monte Carlo calculations are addressed. The potential influence of the dielectric discontinuity between the DNA and solvent and the implications of dielectric saturation around DNA are examined. Results of studies on the structure and equilibrium properties of NaDNA solutions in the absence and presence of excess Na^+Cl^- salt are presented and discussed. We find in all cases a concentration of counterions near DNA (~10 Å) that is in excess of 1 M even in the absence of excess salt, consistent with previous theoretical studies. A comparison of the simulation results on the basis of different dielectric models for the solvent showed that the effects of dielectric saturation on the total energetics, the internal energies of counterion binding, and the local counterion distributions are significant. Saturation favors increased counterion condensation relative to the coulombic model, with DNA–counterion interactions dominating the small ion repulsions. A consideration of the lowering of the solvent dielectric constant near DNA and near small ions due to dielectric saturation in water results in an essentially salt-independent estimate of the net counterionic charge per phosphate around DNA over the added salt concentration range of 25–150 mM studied here. This observation is also consistent with the counterion condensation theory and the current inferences from ^{23}Na NMR experiments.

I. Introduction

Polyelectrolyte effects play an important role in many aspects of the structure and function of nucleic acids.[1-3] The counterion atmosphere of DNA neutralizes the charges of the anionic phosphates and imparts electrostatic stability to the system. The nature of this effect, "counterion condensation", is unique in polyelectrolytes compared to simple electrolyte systems.[1,2] Release of condensed counterions is considered to be an important thermodynamic component of ligand and protein binding to DNA.[3]

While the significance of counterion condensation is well documented, relatively little is known at the molecular level about the structural details of the organization of counterions around the various forms of DNA and the detailed nature of the electrostatic stabilization. Recently some advances have been made in this direction via Monte Carlo (MC) computer experiments,[4-12] which also point to certain methodological issues of concern in molecular simulations on the basis of the primitive dielectric model for environmental water. A typical problem encountered in these studies is a high acceptance ratio for single-particle Metropolis moves and its commensurate impact on the convergence of the calculated thermodynamic and structural indices. In addition, the role of dielectric saturation and the influence of the dielectric boundary between the DNA and solvent on the potential of mean force between the counterions and the anionic phosphates of duplex DNA are issues not fully resolved.

In a series of studies reported recently,[13-15] the structural features of water around DNA as a function of conformation and base composition have been characterized via MC simulations and calculated hydration densities and compared with available experimental results. We describe herein complementary MC studies of the counterion atmosphere of B-DNA, focusing particularly on issues of detailed structure underlying counterion condensation. Previous MC studies on ion atmosphere from diverse laboratories[4-12] have considered only the radial distribution of the counterions. The effect of excess Na^+Cl^- salt on the results in the concentration range of 0–150 mM is also considered.

II. Background

The nature of the ion atmosphere of DNA has been the subject of considerable research attention, both experimental and theoretical, in recent years. An important organizing principle is the phenomenon of "counterion condensation" (CC):[16] no matter how dilute the solution, a number of the counterions remain in close proximity to the DNA, compensating a large percentage of the phosphate charges, and are said to be "condensed". This follows simply from thermodynamic arguments. Small ion pairing is well-known to decrease with dilution due to the increased potential for a large entropy of mixing, which favors dissociation. For polyions, the superposition of the electrostatic potentials of the phosphate groups on any given mobile counterion makes enthalpic effects dominant in the equilibrium, and as a consequence a significant fraction of counterions remain associated with the DNA regardless of the bulk salt concentration.

In a series of papers, Manning[1,17-23] analyzed the problem and came to the vexingly simple conclusion that the percent condensation of monovalent mobile cations on DNA was simply 76% (88% for divalents) and indepen-

0024-9297/90/2223-3156$02.50/0

dent of salt concentration. This result was obtained from theoretical studies in which DNA was treated as a line of charges. The remaining mobile ions form a less concentrated distribution around the screened charges and were treated by a Debye–Hückel approach. An entropy of mixing term completes the picture. Minimization of free energy resulted in net phosphate charges screened from −1 to −0.24 by the condensed monovalent counterions. Manning has provided an account of diverse observed properties of DNAs via counterion condensation theory.[1,23]

An alternative theoretical approach to the problem is based on solutions to the Poisson–Boltzmann (PB) equation for simplified models of DNA.[24-30] Zimm and LeBret[28] showed elegantly using the PB equation how a rodlike polyanion like DNA on increasing dilution will naturally condense counterions at a level intermediate between that of a charged sheet (100% condensation, the Gouy Chapman double layer) and that of a charged sphere (~0%). Elaboration of the PB treatment of ion atmosphere has been advanced considerably by Record, Anderson, and co-workers.[26,27,29] They have investigated numerous aspects of the problem vis-à-vis thermodynamic measurements and NMR spectroscopy, with a focus on the salt dependence of the fraction of the condensed counterions. Their Poisson–Boltzmann cell model studies and their grand canonical Monte Carlo predictions of the "preferential interaction coefficient", which they identify as a thermodynamic measure of nonideality due to small ion–polyion interactions, have provided a considerably enhanced perspective on the problem.[8-10] In these calculations, limitations of the PB theory due to neglect of finite size of the mobile ions and spatial correlations have been a matter of concern[6-8] and have been characterized by comparisons with MC calculations in several groups[4-12] and with HNC theory.[31] Qualitative agreement among the various theoretical methods has been reached, although it has been shown that the PB approach underestimates the counterion concentration by 12–18% close to the DNA[5] as described by a charged cylinder. Both PB and MC calculations have been used to investigate Manning's CC theory prediction about the insensitivity of charge compensation of phosphates to added salt concentration and found in fact slight but potentially significant variation.[4-12]

Recently the theoretical studies of ion atmosphere have been extended to treat all-atom models of DNA.[32-34] Klein and Pack[32,33] obtained electrostatic potentials from an iterative PB solution to a combination of Coulombic potentials from the fixed macromolecular charges and the distribution of mobile charges obtained from the Boltzmann equation. The results also predict significant concentration of mobile cations in the minor groove as well as along the sugar phosphate backbone, a consequence of the superposition of transgroove anionic phosphate potentials. However, this treatment assumes $\epsilon = 80$ everywhere including inside the DNA.

The potential influence of the dielectric boundary between the DNA (ϵ = 2–4?) and solvent at $\epsilon \sim 80$ was recently explored by several groups.[35-38] Troll et al.[37] conducted a macroscopic simulation of duplex DNA represented by a clay model in an electrolyte tank. The electrostatic potentials obtained from these clay model simulations were subsequently employed in a Monte Carlo determination of counterion distributions around DNA.[11] It was found that (a) interactions of ions on the same side of the DNA were enhanced as a consequence of a concentration of field lines by the low dielectric DNA, increasing both attractive phosphate–cation and repulsive cation–cation interactions and (b) shielding is increased for charges on opposite sides of DNA by the presence of the low dielectric medium. The net effect of the dielectric boundary on the system is a diminished tendency for the residency of cations in the grooves of the double helix. Jayaram, Sharp, and Honig[38] have more recently incorporated dielectric boundary, solvent screening, and ionic strength into finite difference solutions to the PB equations (FDPB)[39,40] for an all-atom model of DNA. The numerical results qualitatively support the electrolyte tank observations on the angle dependence of the charge–charge interactions. In contrast to the tank results, FDPB calculations show an overall increase in the groove populations of counterions at low ionic strengths. Both of these studies underline the importance of the dielectric boundary in rigorous descriptions of the DNA environment. However, in all the above quoted studies, solvent water is treated as if the dielectric constant was everywhere equal to the bulk value of ~80.

Dielectric inhomogeneity and the influence of dielectric saturation on oligonucleotide–small ion interactions has been studied by Hingerty et al.[41] by means of a distance-dependent dielectric screening function, subsequently employed in energy minimization studies on DNA by Lavery and co-workers using the JUMNA method.[42] Troll and Zimm[43] studied the influence of dielectric saturation around a cylinder-shaped DNA model using the Poisson–Boltzmann method. They concluded that saturation results in a somewhat steeper counterion concentration gradient and higher surface counterion concentration but does not markedly affect the bulk thermodynamic properties. These inferences, however, do not apply to DNA-shaped molecules with groove structure, where the situation is still unclear. This possible lowering of the solvent dielectric constant in the grooves has not been considered so far in any of the simulation studies reported on counterion distributions around DNA.

An additional point of interest is the structure (or lack of it) assumed by the counterions within the region of condensation. This is of considerable importance in diverse areas such as salt effects on protein–DNA interactions and the development of a suitable initial configuration for the treatment of counterions in molecular dynamics (MD) simulation studies on nucleic acids. Considerable ambiguity exists with regard to underlying structural details of the ion atmosphere. Manning[1] is careful to distinguish condensation (i.e., remaining associated with the DNA) from actual site binding. NMR experiments have been cited in support of the idea advanced in ref 1, that "all small cations are in a state of complete hydration and free translational and rotational mobility", i.e., delocalized and rather loosely associated with the DNA. The Manning radius (of the counterion condensate) is typically ~17 Å.[1] On the other hand, the duplex rotation angle of DNA has been found to vary systematically with cation type,[44] which may require an explanation involving some degree of site binding. Multivalent cations seem to be more disposed to site binding than monovalents.[45] Results on counterions in nucleic acid systems from X-ray crystallography are fragmentary.[15]

The NMR literature is quite extensive on cation resonance in DNA systems.[46-50] Experiments involving ^{23}Na NMR indicate support in large measure to the condensation hypothesis,[48] but the data have proved to be difficult to interpret unequivocally in terms of structure. Also the exact nature of the quadrupole relaxation mechanism of the sodium nucleus via electric field gradients is not clear. Record, Anderson, and co-workers[48] speak of a relaxation mechanism involving radial diffusion, sen-

sitive to DNA conformation but not composition. A recent theoretical analysis by Reddy, Rossky, and Murthy[51] points to relaxation via ion motion in the vicinity of the polyion electrostatic potential, with negligible contribution from radial diffusion. More recently Bacquet and Rossky[52] estimated mean-square electric field gradients from HNC studies of ion distributions around DNA and found a very good correlation with measured NMR line widths. Their analysis is based on a two-state view of the counterions and is consistent with the ideas advanced earlier.[1,48] There is still some uncertainty with regard to the character of the diffusional motion dominating the relaxation mechanism and the extent of counterion association.

We describe herein studies aimed at pursuing the nature of the ion atmosphere of DNA further based on molecular simulation. There are basically two options: (a) simulations using variations on the primitive model in the vein of refs 4–12 or (b) Monte Carlo or molecular dynamics calculations based on a fully explicit consideration of DNA, water, and counterions. Previous simulation studies[53–55] of the latter type have led to contradictory results on the ion distributions.[54,55] We report herein our progress in the area of option (a), with variations on the restricted primitive model. We also have some extensive molecular dynamics simulations of type (b) in progress that will be completed soon and reported shortly.

In the primitive model, ions are treated explicitly and water is represented as a dielectric continuum. This is clearly a serious approximation since the molecular nature of water as an associated liquid is neglected and its particular capacity for hydration, bonding, and solvation in different modes—hyrophilic, hydrophobic, and ionic—is denied. Also, there is no way to accurately parametrize the heterogeneous qualities of the dielectric medium from experimental data. Thus, we have taken up comparative simulations of the counterion distribution around DNA based on a series of models for aqueous dielectric medium which are likely to bracket the true physical nature of the system. Subsequent comparisons of the results of the aqueous dielectric models with fully explicit simulation studies are planned to ascertain further the relevance and applicability of the various models.

III. Calculations

Statistical thermodynamic (T, V, N) ensemble Monte Carlo simulations were first carried out on dilute aqueous solutions of NaDNA at a temperature of 300 K, using Metropolis sampling procedures.[56] The system for study consisted of two turns of DNA with 40 negatively charged phosphate groups and 40 sodium counterions enclosed in a cylinder of radius 50 Å. The central cell of the simulated system thus corresponds to an electrically neutral solution of a 20mer of NaDNA, fixed in the canonical B-form, ~3 mM in DNA concentration and ~120 mM in Na^+. The mole fractions $x_{Na^+} = x_{PO_4^-}$, and we refer to this condition of minimum compensating sodium as "zero added salt".

The N-particle configurational energies of the system are calculated under the assumption of pairwise additivity in intermolecular interactions using 12-6-1 atom site potentials to describe both the sodium–phosphate and sodium–sodium interactions. The general expression for the pairwise interaction energy between sites i and j is

$$V_{ij}(R) = \frac{C_{12}}{R_{ij}^{12}} - \frac{C_6}{R_{ij}^{6}} + \frac{C_{ij}Q_iQ_j}{\epsilon(R_{ij})R_{ij}} \qquad (1)$$

where C_{12} and C_6 are the Lennard-Jones repulsive and attractive parameters, the Q_i's are the electrostatic charges,

Table I
GROMOS Lennard-Jones Energy Function Parameters Used in This Study

atom/ion	C_6, kcal·Å^6	C_{12}, kcal·Å^{12}	Q
P	3522.4225	5 303 809	−1
Na	17.2225	5 022.5569	+1
Cl	3299.3536	25 553 025	−1

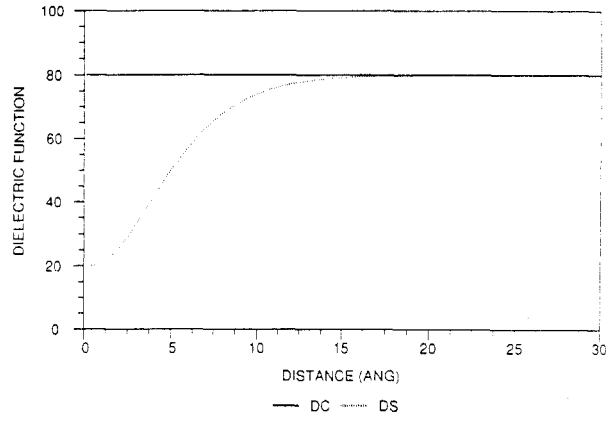

Figure 1. Illustration of the dielectric function (DS model) adopted in this study to examine saturation effects.

C_{ij} is an electrostatic modulation factor, $\epsilon(R_{ij})$ is a dielectric screening function, and R_{ij} is the intersite distance of separation. The 12-6-1 parameters employed in this study (Table I) are adapted from the GROMOS force field and for the cation correspond to those of unhydrated sodium ion. A geometrical mean of the parameters of the ions involved is used in calculating the 12,6 interaction energies. For example, the C_{12} parameter for the interaction of Na with P is derived as $(C_{12}^{Na}C_{12}^{P})^{1/2}$. Solvent is treated as a modified homogeneous dielectric continuum.

Four prescriptions are examined in evaluating the electrostatic contribution to the sodium–phosphate interactions: (a) model DC, the Coulombic potential with C_{ij} = 1 and $\epsilon(R_{ij})$ = 80; (b) model DD, a modified coulombic potential incorporating the effects due to dielectric discontinuity in the small ion–polyion interactions using the data of Conrad et al. for C_{ij}'s (Table I of ref 11) with $\epsilon(R_{ij})$ = 80 (The repulsive energy of interaction of a small ion with the low dielectric DNA and the discontinuity effects in small ion-small ion interactions are not included in this model.); (c) model DS, using a modified Hingerty function[41,42] for the $\epsilon(R_{ij})$ to include effects due to dielectric saturation, with C_{ij} = 1; (d) model DS/DD, a combination of models b and c, i.e., a modified $\epsilon(R_{ij})$ as in DS model and C_{ij}'s as in model DD.

The behavior of the dielectric function (DS model) adopted in this study as a function of interionic distance is shown in Figure 1. This function describes the scaling factor for interactions between DNA and counterions in aqueous medium relative to vacuum. It may be noted from Figure 1 that at very short distances between two ions, the dielectric function DS takes a value of 20. At very long distances this function goes smoothly over to a value of 80. A midvalue of 50 is attained at a charge to charge separation of ca. 5 Å. To maintain consistency, the same $\epsilon(R_{ij})$ function is used to treat both the DNA–counterion and counterion–counterion interactions in the simulations using the DS and DS/DD models. One justification for the usage of a dielectric saturation function comes from the observation that electric fields around ions are on the order of a million volts per centimeter.[57] The fields near polyions such as DNA are even larger and are expected to reduce the dielectric con-

stant of the solvent within the vicinity of the polyions. Figure 1, however, must not be construed as a quantitative description of the dielectric properties of the solvent around DNA. Also see ref 58 for a simulation study on small ion hydration in this regard, where it is concluded that saturation may be important only beyond a charge of +1 for cations. There is no clear information on the dielectric constant of the solvent around DNA. As already stated in the Introduction, these models (a–d above) are investigated here with the hope of bracketing the true physical nature of the system. Calibration studies of the dielectric function via fully explicit MD simulations and grand canonical Monte Carlo simulations are also in progress.

The structure of our DNA is generated from the local coordinates of Arnott and Hukins[59] and corresponds to the canonical B72 form of the sequence d(GCGAATTCGC)$_2$. A charge of −1 (in atomic units) is placed on the phosphate at the location of the phosphorus atom that is closest to the charge center of the phosphate group, in keeping with the model of Zimm and co-workers.[11,37] The solute in our simulations thus corresponds to simply a DNA-shaped molecule with charges on phosphates. Counterions are prevented from penetrating into the DNA interior by means of a repulsive step function added to the configurational energy.

Periodic boundary conditions along the helical axis and mass conserving diffusive boundary conditions in the radial direction are imposed on the system. For instance, if a counterion moves out of the cylinder radially to (r, ϕ, z), it is repositioned at $(r', 180 + \phi, z)$. Here r' is given as $d - r$, where d is the diameter of the outer cylinder (100 Å in this study). Similarly, in the axial direction if the particle diffuses out of the cylindrical box to (r, ϕ, z), it is reset at $(r, \phi, z - h)$, where h is the height of the cylinder. In our case h is 67.6 Å. All the interactions inside the central cell are treated under minimum image convention along the axial direction. The end effects in our model are dealt with as follows: When the coulombic part of the interaction energies of a small ion with DNA and with other small ions are calculated, one image of the central cell in either direction along the helical axis is included, with the central cell for the ion under consideration created in a minimum image convention.[60] End effects mean here and in the following the effects due to a consideration of the finite-sized cell, and these do not refer to oligomeric end effects.

The contribution of the two image cells in our calculations to the interaction energies is of the order of 3–6% of the total energies for the different models investigated here. Accepting this limit obviates the need to use external potentials to describe the small ion interactions and ensures that small ion–polyion and small ion–small ion interactions are treated in a similar manner. A combination of logarithmic potential for small ion–polyion interactions with external potentials for small ion–small ion interactions was used in related previous studies.[5,6]

The explicit evaluation of all the interactions along the axial direction up to one image cell in either direction contributes to the superimposed anionic potentials which give rise to the polyelectrolyte nature of DNA. No images are created in the radial direction. The motivation for this is to circumvent the need to specifying cutoffs for the small ion interactions and the inherent problems of a slowly decaying r^{-1} potential and to remove any bias toward condensation of counterions due to the repulsion of the central cell counterions that would be introduced by radial images.

The Monte Carlo sampling applied in this study proceeds according to the Metropolis prescription,[56] which involves optimizing the sampling of configuration space and hence convergence via important sampling consistent with Boltzmann statistics and microscopic reversibility. In the Metropolis method, the stochastic walk proceeds according to an acceptance–rejection criterion based on the energy differences of sequential configurations generated by random changes in the positions of the particles of the system. In the Metropolis method, a balance is struck between two extremes, large changes where the probability of rejection is high due to van der Waals overlaps (clashes) and small ones where insufficient new information is obtained to significantly advance the sampling.[61]

In most Monte Carlo studies of molecular assemblies, such as liquid water at liquid densities, a strategy is defined by the translational and orientational displacement of a single particle. The balance is achieved by adjusting the step size for this particle to attain a 50% acceptance rate, which produces satisfactory convergence. The application described here involves a particle density of 7.53×10^{19} ions/cm^3 compared to the liquid water value of 3.35×10^{22} molecules/cm^3. In such a dilute system, the step size in a single-particle move to achieve 50% acceptance rate is quite large due to the fewer opportunities for clashes. The Monte Carlo calculations of ions in a dielectric around charged cylinders as well as previous DNA models have thus used large translational displacement. In the case described by Murthy et al.,[5] a step size of 100 Å still only led to a 65% acceptance rate. The convergence properties for the ion–DNA radial distribution functions were seen, however, to be satisfactory.

In this study the information we seek is on the detailed spatial and orientational distribution of ions in the immediate vicinity of DNA where the characteristic length is of the order of angstroms. The displacements involved in single-particle moves would obviously be an inefficient way to obtain this information, and the structural details underlying the radial distributions would be expected to converge very slowly. Thus we maintained individual displacements arbitrarily at 1.5 Å and turned to a strategy of "multiple-particle moves"[62] to achieve 50% acceptance. Multiple-particle moves here imply that more than one particle is attempted for movement during a Monte Carlo step. Exploratory calculations showed that a 50% acceptance criterion was achieved with 8–10 particle moves (for DC and DD models and 2–3 particle moves for DS and DS/DD models), where the particles are chosen by a shuffled cyclic method.[63] The components of the displacement vector $(\delta x, \delta y, \delta z)$ in cartesian space for each ion to be moved are obtained by uniformly sampling the domain D ($D = \Delta r^3$) located at the center of each ion situated at (x, y, z) and defined by the step-size parameter Δr, which is equal to 1.5 Å in the present study (also see ref 64 for details on the calculation of the displacement vector). All simulations reported herein are based on the Metropolis method with 1.5-Å displacements and multiple-particle moves, with the number of particles per move optimized for the convergence of calculations based on a specific dielectric model.

Convergence of the Monte Carlo runs was monitored by defining block averages on the average internal energy of the system and the volume integral of the net charge density in a cylinder of radius 20 Å around DNA. The latter was found to be slower to converge than energy during preliminary studies. Some 75 000 passes are generated for each run. A "pass" here refers to as many single-

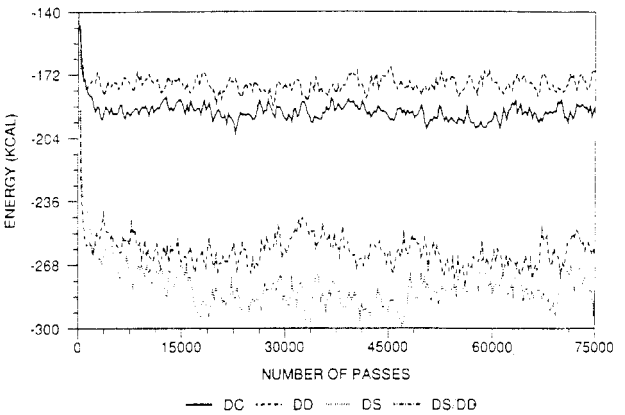

Figure 2. Convergence profiles of block averages of energies as a function of run length in passes for different dielectric models. Block size is 250 passes. Each pass is equivalent to 40 single particle moves (at zero added salt): solid line, DC model; dashes, DD model; dots, DS model; dash-dots, DS/DD model.

particle moves as there are particles. Thus with 40 mobile ions at zero added salt, 75 000 passes is the equivalent of (40 × 75000) 3 million configurations for single-particle moves. The convergence profiles for the block averages of the total internal energies and the net counterion charge per phosphate in a cylinder of radius 20 Å around DNA are shown in Figures 2 and 3 and are seen to be stable. Beyond 20 Å, the electrostatic potential is relatively independent of the DNA model,[38] and there is no noticeable further structure in any of the calculated radial distribution functions of counterions. Thus, a radius of 20 Å was chosen for monitoring convergence of the counterion distributions. The first 25 000 passes (corresponding to 1 million single-particle configurations) of each run are treated as equilibration and discarded. Ensemble averages were formed over the last 50 000 passes (referred to as the production segment below) of each simulation.

IV. Results

The average total internal energy and the counterion fraction up to a distance of 20 Å from the helical axis are reported in Table II, along with statistical uncertainties up to 95% confidence level. The DD model is the highest on the enegy scale, followed by the DC model and the DS/DD model. The DS model gives the lowest energy. This ordering is intuitively quite reasonable. The calculated internal energies are correlated to the number of counterions per phosphate residing in the vicinity of DNA (column 4 of Table II) with a correlation coefficient ≤ -0.7. The DD model gives the lowest and the DS model the highest number of counterions in any given volume close to DNA. The influence of dielectric discontinuity is smaller than that of dielectric saturation. The results of the DS/DD model indicate that the effects of dielectric discontinuity on DC and DS models are similar as expected.

The radial dependence of the integrated counterionic charge–phosphate around DNA, denoted $q^+(R)$, is shown in Figure 4. The details seen in the curves in Figure 4 below 10 Å are due to the groove potentials manifested via the cylindrical grids for the C_{ij} data.[11] These curves would be much smoother if a finer grid or an all-atom treatment of DNA was used, which is under separate investigation. At least three distinct regions are noticeable in the behavior of $q^+(R)$: the groove region (below 10 Å), the backbone region ranging from 10 to 13 Å for the DS model, from 10 to 15 Å for the DC model, and from 10 to 17 Å for the DD model, and a third region representative of the rest of the system, where the net charge

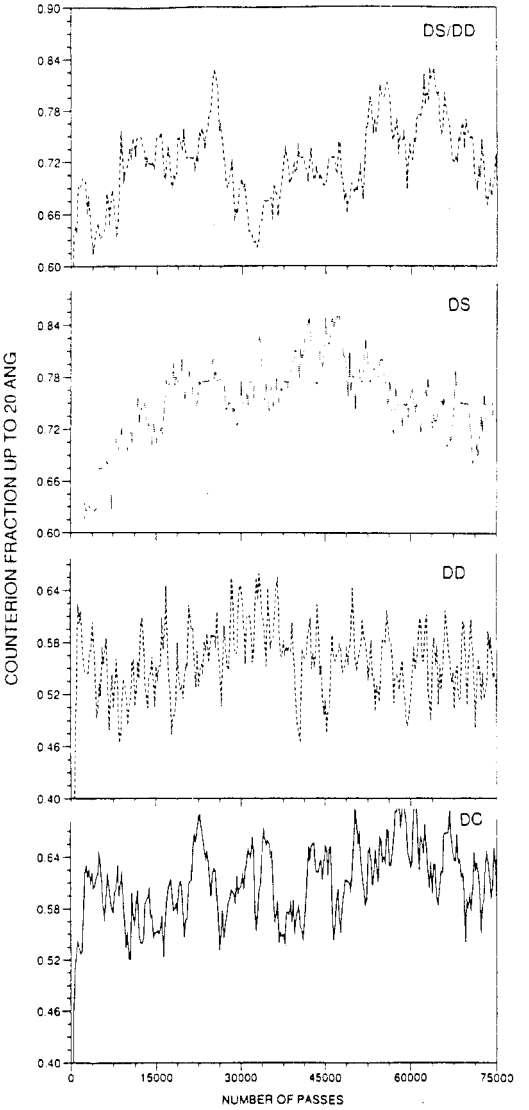

Figure 3. Convergence profiles of block averages of the number of counterions–phosphate (up to 20 Å from the helical axis) as a function of run length for different dielectric models. Block size is 250 passes: solid line, DC model; dases, DD model; dots, DS model; dash-dots, DS/DD model.

Table II
Results of MC Energetics (in kcal/mol) and Condensed Counterion Fraction up to 20 Å Based on the Various Dielectric Models

model	$\langle E \rangle$	$\pm 2\sigma$	$\langle$CCF$\rangle$	$\pm 2\sigma$
DC	−191.52	1.33	0.619	0.016
DD	−177.12	0.89	0.564	0.012
DS	−281.96	2.62	0.767	0.018
DS/DD	−274.95	3.73	0.717	0.024

increases monotonically with distance. The demarcations are particularly pronounced with the DS model. In the DS model, Manning's fraction of 0.76 for the counterions is achieved at a distance of ~17 Å, in reasonable accord with his analysis. The inflection points on the curves in Figure 4 and the corresponding counterionic charge per phosphate up to the inflection point are collected in Table III. These are determined by extending the two straight line portions of each curve to an intersection point and by drawing a bisector from the intersection point to the curve. Figure 4 and preliminary calculations with a larger cylinder of radius 100 Å also show that the counterion distribution near DNA is not significantly influenced by the presence of the outer boundary at 50 Å.

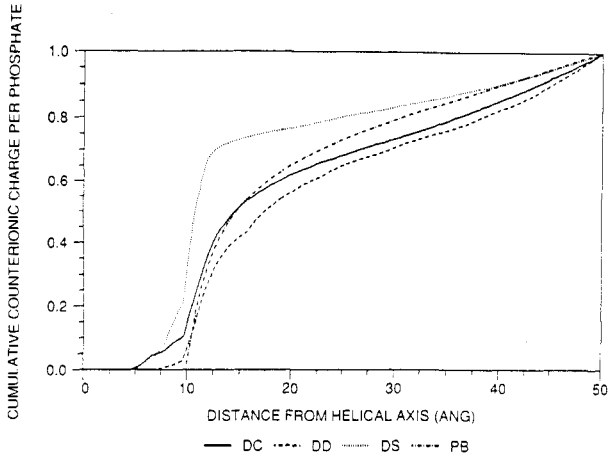

Figure 4. Cumulative counterionic charge per phosphate at zero added salt shown as a function of distance from the helical axis: solid line, DC model; dashed line, DS model; dotted line, DD model; dash-dot, the cylindrical PB approach.

Table III
Inflection Points R_i and Integrated Counterion Fraction per Phosphate $q^+(R_i)$ up to the Inflection Point

model	distance (R_i), Å	$q^+(R_i)$
DC	15	0.52
DD	17	0.48
DS	13	0.70

The results from a PB treatment of the counterions are also shown in Figure 4, calculated by solving the nonlinear Poisson–Boltzmann equation[26] for a cylinder of radius 10 Å enclosed in an outer cylinder of radius 50 Å with $\epsilon(R_{ij}) = 80$. The PB equation slightly underestimates the counterion concentrations compared with the DC model at distances below 15 Å, from DNA consistent with previous observations.[4-6] The effects of the inclusion of small ion correlations and the finite size of the counterions are small as pointed out earlier.[4-8,24] Finite ion size and ion–ion correlations have opposing effects on the distribution of counterions around DNA, which must partially account for the success of the simple continuum models.

The counterion probability densities are shown in Figures 5–7. This analysis scheme is analogous to that used for the description of hydration density around DNA reported earlier.[13,14] The calculated spatial distribution of the counterion density is depicted for presentation here as the linear superposition of points representing the counterions from a series of 20 configurations chosen at equally spaced intervals along the production segment of the Monte Carlo realization. Any individual point simply indicates that a counterion is present in one or another of the ion configurations contributing to the statistical state of the system. The important information conveyed by this figure is the clustering of points, indicating a concentration of counterion density in that region. Note that the circles in Figures 5–7 represent about 62%, 56%, and 77% of the counterions, respectively, in the system (also see Table II). Full circles represent counterions in a cylinder of radius 12 Å enclosing the DNA. Open circles represent counterions in a coaxial cylinder from 12 to 20 Å around DNA. Figures 5 (DC) and 6 (DD) show a more diffuse arrangement of the counterions along the length of DNA relative to Figure 7 (DS) where the counterions are densely populated along the backbone of DNA.

The simple coulombic model (DC model) gives a highly dispersed mobile ion density, with considerable groove as well as backbone populations. The net effect of incorporating dielectric discontinuity using the C_{ij} data of Zimm and co-workers[11,37] is an overall decrease of the attraction of DNA for the counterions, particularly the groove regions. On introducing the dielectric saturation, the DNA and the backbone regions in particular are found to be much more attractive to counterions.

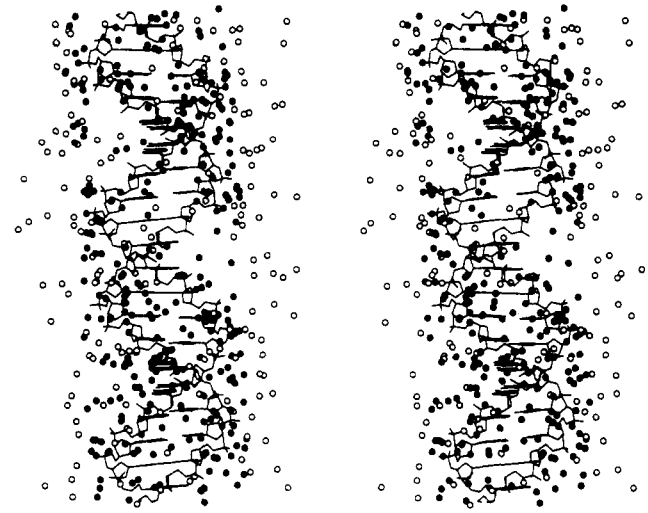

Figure 5. Stereoviews (proximal views) of the counterion probability density around DNA for the DC model based on the superposition of 20 snapshots obtained at equally spaced intervals in the simulation. Full circles represent counterions in a cylinder of radius 12 Å enclosing the DNA. Open circles represent counterions in a coaxial cylinder from radius 12 to 20 Å around DNA.

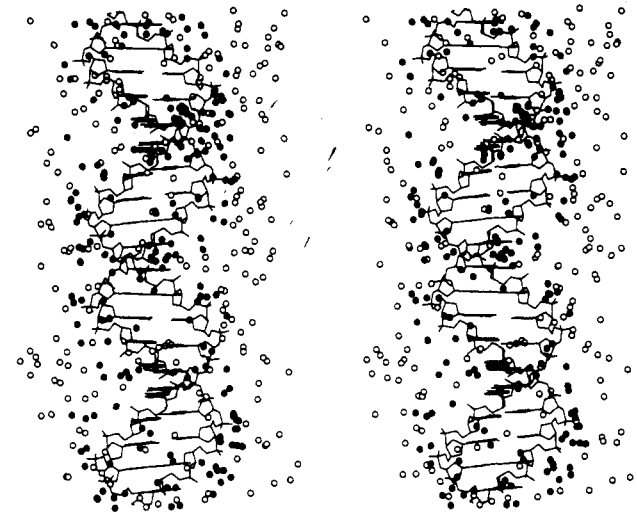

Figure 6. Stereoviews (proximal views) of the counterion probability density around DNA for the DD model. Circles represent counterions as in Figure 5.

We have also carried out MC simulations on the three different dielectric models (DC, DD, and DS) at 25, 50, 100, and 150 mM added salt (NaCl) concentrations. The salt dependence of the net counterionic charge within the vicinity of DNA is of interest in the light of ^{23}Na NMR experiments.[46-48,50] The results for the net positive charge per phosphate in a cylindrical shell of 20 Å around DNA are shown in Figure 8a as a function of salt concentration. The added salt concentrations studied correspond to a sodium/phosphate ratio [Na]/[P] of 1.2, 1.4, 1.8, and 2.2, respectively. The salt-independent estimate of 0.76 of the CC theory is shown as a continuous solid line. All three models show a nonzero slope over the salt concentration range of 0–25 mM. As the salt concentration is increased further, the results from the DS model quickly stabilize to a salt-independent value of 0.815 ± 0.005, while the results of the DC and DD

Figure 7. Stereoviews (proximal views) of the counterion probability density around DNA for the DS model. Circles represent counterions as in Figure 5.

models are still changing. A choice of a radius smaller than 20 Å shows even less dependence (Figure 8b) of the integrated net counterionic charge on the added salt for all the three models. The DS results seem to be the first observation of Manning-type salt independence of $q^+(R)$, over the salt concentration range studied, in a primitive model system.

For comparison purposes, the counterionic fractions calculated from the electrostatic potentials, obtained by using the FDPB method[38-40,65] as solutions to the nonlinear Poisson–Boltzmann equation incorporating dielectric discontinuity, are shown in Figure 8c. The FDPB results (particularly at 20 Å) are similar to the saturation DS model results (see Figure 8a), but since they are based on quite different physical models, this observation is intriguing. This is addressed further in the following section.

V. Discussion

The Monte Carlo simulations based on all variations of the primitive model considered here show a concentration of counterions near DNA (~10 Å) that is in excess of 1 M even at zero added salt concentration. There is a strong tendency for the counterions to populate regions proximal to DNA, whatever the bulk salt concentration, consistent with the observations emerging from earlier theoretical studies on DNA–counterion systems. Dielectric saturation increases this tendency and also leads to a decrease in dependence of the net counterionic charge around DNA (≤20 Å) on added salt concentration.

When we relate this work to earlier studies,[4-6,11] some methodological differences involved and their implications must first be considered. The simulations reported here are carried out over much longer run lengths than those reported previously on DNA–counterion systems. The DC model here is comparable to that in refs 4–6 and the DD model to that of Conrad et al.[11] except for the use of ionic radii corresponding to hydrated sodium ions for those far from DNA and inclusion of repulsive interactions between counterions and low dielectric DNA in their work. A number of previous studies treat the DNA as a uniformly charged cylinder and use a limiting logarithmic form in computing the DNA–counterion interactions. The logarithmic potential does not reflect the presence of distinct regions in $q^+(R)$ noticeable with discrete phosphate charges and groove structure. Also if

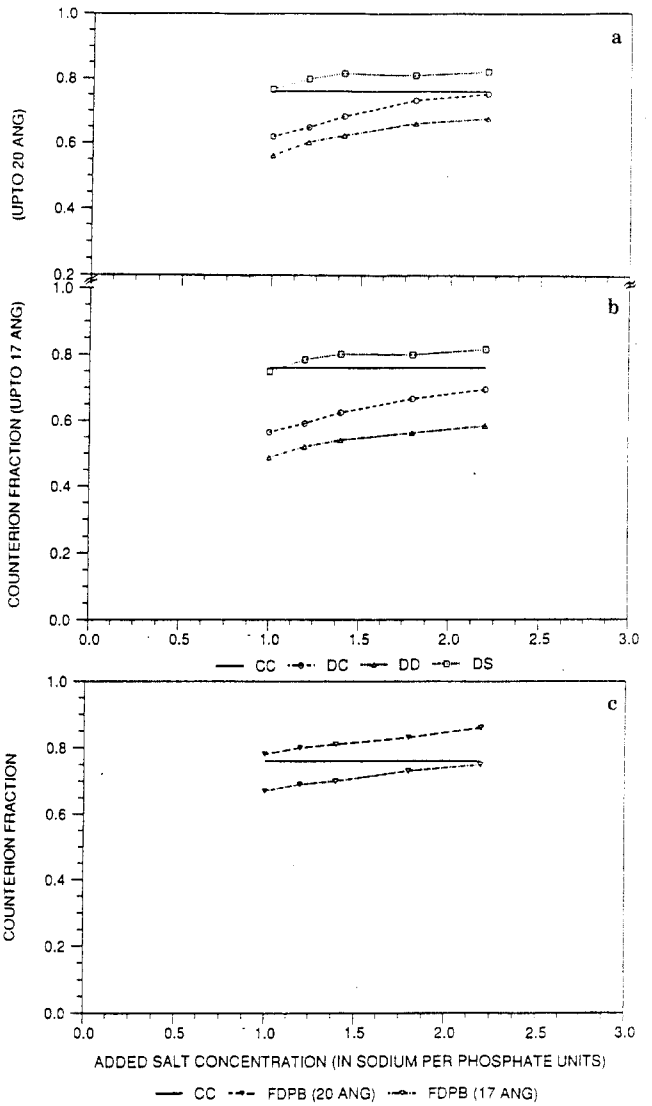

Figure 8. Net counterionic charge/phosphate integrated up to a distance of (a) 20 and (b) 17 Å, from the helical axis versus added salt concentration shown as the ratio [Na]/[P]. [Na]/[P] = 1 refers to zero added salt condition: solid line, CC theory; circles, DC model; triangles, DD model; squares, DS model. (c) Results from the FDPB method for a condensed counterion fraction up to 20 Å (dash, inverted triangles) and 17 Å (dash-dots, inverted triangles).

the polyion–small ion interactions and the small ion–small ion interactions are treated differently[5,6] as is the case when the logarithmic potential is taken for the former and a minimum image convention for the latter, an imbalance is created in the number of interactions, leading to an overestimate of the polyion–small ion interactions. To correct for this, an external potential[5,6] has been required. The extent of errors introduced by such an approach has not been estimated but should be small. In our studies the true helix shape and groove structure of B-DNA duplex are taken into account, and the logarithmic form is not applicable. Other limitations due to end effects and periodic boundary conditions do arise.

We have been able to estimate the contribution of the end effects in our calculations to the free energy of counterion assembly by means of a perturbation procedure[66] used to evaluate the free energy difference between the system with and without contributions from image cells. This free energy difference turned out to be 9.30 kcal, with ΔE = 9.73 kcal and $T\Delta S$ = 0.43 kcal. The entropy term is positive as expected, reflecting a loss of order due to a partial removal of the correlations between the

small ions. The contribution of the entropic term is only about 4.4% of the internal energy term. This analysis provides an estimated upper bound in the energy due to correlations introduced by the present treatment of the end effects.

The nature of the periodic boundary conditions in the radial direction employed in this study constitutes another departure from the work reported earlier.[5,6] A mass-conserving diffusive boundary is employed here as an alternative to the constraint (hard-wall) potential at the boundary of the cylinder. A hard wall may create an attractive potential[67] at the boundary.

We now proceed to examine the similarities and differences in the results given the above differences with the work reported earlier. A net counterionic charge per phosphate, integrated up to 7 Å from the surface of the DNA, is inferred from the calculations of Record and co-workers in Figure 7 of ref 6 to be 0.55, at zero added salt. In our results, the corresponding value can be read from Figure 4 for a distance of 17 Å (10 Å for the radius of the DNA + 7 Å beyond) to be 0.57 for the DC model. The DD and the DS models give results that differ from this value considerably, as seen from Figure 4. The results of Murthy et al.[5] are not directly comparable to ours as all their simulations are at nonzero added salt concentrations. Taking their simulation at the lowest salt concentration (0.001M), a value of 0.62 at 20 Å can be inferred (Figure 4b of ref 5). This differs from our value for the DC model in Table II (row 2 and column 4) only insignificantly. However, their calculated Manning radius for 0.76 counterionic charge is 52.2 Å at this concentration, which is much larger than our "zero added salt" result (see Figure 4).

Conrad et al.[11] reported a value of 0.63 for the net counterionic charge/phosphate (average of the sums of numbers in rows 3 and 4 of Table III of ref 11 divided by the total number of phosphates in their simulation) at a distance of 10 Å from the "exclusion curve" for the model with "simple coulombic energy" corresponding to our DC model. The corresponding number for the "complete electrostatic energy" model, which is similar to our DD model, is reported as 0.58 (from rows 9 and 10 of Table III in ref 11). This indicates that the dielectric discontinuity as incorporated via the C_{ij} data[11,37] results in a depopulation of the grooves and also has the net effect of decreasing the *total* number of counterions within the vicinity of DNA. Identical trends are observed in our DD calculations (see rows 2 and 3 under column 4 in Table II and the Results section). Our calculations indicate that dielectric saturation has a significant effect on the total energetics (as seen from Table II for the DS model) in contrast to the findings of Troll and Zimm.[43] However, both studies agree on the observation that a steeper counterion concentration gradient exists as the dielectric constant is lowered near DNA as expected when saturation is included.

We have also obtained a rough estimate of the free energy difference between the DC and DD models (as an average from DC and DD simulations) using the perturbation method.[66] The free energy difference (ΔA) is evaluated to be 6.35 ± 3.75 kcal/mol for the hypothetical process of converting model DC into DD. The internal energy difference (ΔE) from Table II is known to be 14.40 kcal/mol, giving a $T\Delta S$ contribution of 8.05 kcal/mol for the process DC → DD. The sign of the entropy term is not surprising since, in the DD model, the dielectric discontinuity has the effect of repelling the small ions from the groove regions, which should be favorable entropically. The process DC → DD results in a release of some of the small ions from the grooves. This can also be seen from Figure 4 and column 4 of Table II and further emphasizes tht counterion condensation is enthalpy driven while counterion release is entropy driven.

The sensitivity or lack thereof to ionic strength of the condensed counterion fraction provides another point of comparison for our results vis-à-vis counterion condensation (CC) theory[1] and ^{23}Na NMR.[48] The results on ionic strength dependence for the constant dielectric model (DC) are similar to those observed by Mills et al. (Figure 7 of ref 6). The dielectric saturation model (DS) is seen to show essentially a zero slope as the salt concentration is increased. Bleam et al.[48] demonstrated a two-state approximation in which the observed invariance of the slope of the plot of NMR line widths as a function of salt concentration implies the constancy of the product $r(R_B - R_F)$ where r is the extent of counterion association and $R_B - R_F$ is the difference in the relaxation rates of the bound and free sodium ions. Beyond this, there is some ambiguity in concluding that the two factors r and $R_B - R_F$ are individually constant and in extracting a value for the condensed fraction. (It must be noted that the NMR predictions of the condensed counterion fractions are in the range of 0.65–0.85 from ref 48 and around 0.53 from a recent study.[50] In both cases, however,[48,50] a constancy of the condensed fraction is implied.)

Previous MC and PB studies[6] with constant dielectric (as in the DC model here) were found to disagree[3] with NMR inferences[48] and with CC theory in particular on two counts. First, the estimated compensated charge fraction of phosphates, for any reasonable choice of the cutoff radius from the surface of DNA, was smaller than the CC theory prediction of 0.76 at zero added salt. Second, both the MC and PB approaches showed ionic strength dependence for the net counterionic charge/phosphate within the vicinity of DNA (a nonzero slope for DC model in Figure 8; also see Figure 7 of ref 6). In this sense, the results from the DD model are less consistent with the predictions of condensation theory than the results obtained from the simple coulombic model (DC). The DS model here differs significantly from the DC model on both counts, giving a higher value for the net counterionic charge around DNA and a relative independence of this quantity over the salt concentration range studied. The FDPB method gives a larger condensed counterion fraction and a smaller slope than the simple coulombic model (Figure 8). This suggests that some level of dielectric saturation and discontinuity may be necessary for the results of the theoretical treatments of nucleic acid systems to correspond to the interpretations of ^{23}Na NMR experiments.[46-48,50]

The differences in the condensed counterion fraction and its ionic strength dependence among the diverse models investigated here may be explained in terms of how the various interactions are described by the different dielectric models. These interactions in decreasing order of importance are as follows: (i) the phosphate–small ion interaction, (ii) the image or the self-energy interaction of the small ion with the low dielectric DNA, and (iii) the small ion–small ion interaction. Taking the simplest model, the DC model, as our reference point, interactions (i) and (iii) are treated with a uniform of dielectric of 80 and interaction (ii) is absent. By contrast, the FDPB potentials,[39,40] due to the self-consistent nature of the solutions, include the effect of the dielectric discontinuity on all three interactions mentioned above within

the limitations of neglecting the small ion correlations. In the DD model, the effect of the low dielectric DNA on the phosphate–small ion interaction is accounted for through the use of the C_{ij} values of Zimm and co-workers.[11,37] Around most of the DNA these are less than 1, an effect they attribute to shielding by the low dielectric DNA. This has the effect of reducing the ion–phosphate interaction, thus reducing the condensed counterion fraction relative to the DC model. Honig and co-workers[38,65] found that these C_{ij} values are underestimated due to zero boundary conditions implicit in the use of the electrolyte tank method. Thus in the FDPB method the phosphate–counterion interactions are more attractive, leding to a higher condensed fraction than in the DD model. At higher salt concentrations, however, the phosphate–counterion attraction is effectively screened, and the ion–self-energy and ion–ion energy terms, i.e., interactions (ii) and (iii) above, become significant. The effect of the low dielectric DNA in the FDPB model is to desolvate and thus repel the counterions from the DNA and more from each other. This acts to reduce the condensed fraction at higher salt relative to the DC model and leads to a relatively flatter ionic strength curve than the DC model. The counterion image repulsion effect, i.e., interaction (ii), is included in the simulations of Conrad et al.,[11] where these interactions reinforced the reduction in phosphate–counterion attraction, resulting in less ions in the grooves and more around the phosphates. The ionic strength dependence of the condensed counterion fraction was not examined in their study, but the effect would be to further lower the DD curves of Figure 8. However, it is to be expected that the higher C_{ij} values that are obtained from FDPB calculations would counteract the ion repulsion, resulting in higher condensed fractions and less ionic strength dependence in the DD model than found here. MC simulations using C_{ij} values and ion repulsion energies calculated from the FDPB potentials are currently underway to examine this point.

The FDPB and the DS models give similar results (Figure 8) because the dielectric saturation function in some ways mimics the effects of the dielectric discontinuity. As a counterion gets closer to the phosphate of DNA, in the FDPB model the dielectric discontinuity enhances the phosphate–counterion attraction. Similarly in the DS model, the decrease in the dielectric function with distance has the same effect. This results in a higher condensed counterion fraction for both models. In addition, the lower dielectric increases the repulsions between the counterions in the DS model. The relative effect is greater at higher ionic strengths, tending to reduce the condensed fraction and flatten out the ionic strength dependence curve. While the DS model has no ion image repulsion term, the increased ion–ion repulsion has the same net effect as the dielectric discontinuity does in the FDPB model. They both act to reduce the concentration of counterions close to DNA as the salt concentration is increased.

The results presented here cannot overall be construed as indicative of the superiority of any of the assumed models in describing the nucleic acid systems but do serve to establish, via simulations, empirical relationships between the various models and results as an aid to further understanding of the problem. A calibration of different models is currently being pursued via full-scale molecular dynamics simulations on DNA and counterions with water molecules treated explicitly (Swaminathan, S.; Beveridge, D. L., unpublished material), which will hopefully provide a more rigorous theoretical reference point for comparing different simpler models. Our calculations could be extended to all-atom treatment of the DNA–counterion interactions. In addition, effects of discontinuity in small ion interactions and the repulsive interactions between small ions and the low dielectric DNA can also be considered. However, a limitation of the usage of C_{ij} data of ref 11 and the DD model is that any interpolation scheme is limited in accuracy, and furthermore sequence specificities with an atomic level description of DNA cannot be readily treated. Incorporation of FDPB potentials,[38-40] however, offers an interesting alternative, which is being considered in follow-up studies.

VI. Conclusions

We find in all cases a concentration of counterions near DNA ($\sim$10 Å) that is in excess of 1 M even in the absence of excess salt, consistent with counterion condensation theory and previous Monte Carlo and Poisson–Boltzmann studies on DNA–counterion systems. A comparison of the simulation results based on different dielectric models showed that the effects of saturation on the total energetics, the internal energies of counterion binding, and the local counterion distributions are significant. Saturation favors increased counterion condensation relative to the coulombic model, with DNA–counterion interactions dominating the small ion repulsions. The latter become significant only near the floor of the grooves where the available volume is small and at nonzero added salt concentrations. The DS model produces an essentially salt-independent result for the fraction of condensed counterions, consistent with inferences based on NMR and CC theory. Whether one gets the right answer for the right reason or not remains to be unequivocally established.

Acknowledgment. This research was supported by grants to D.L.B. from the National Institutes of Health (GM-37909) and via the Bristol Myers Corp. and State of Connecticut High Technology Research and Development Award. B.H.'s contribution was supported by grants from NIH (GM-30518) and ONR (N00014-86-K-0483). Supercomputer time was provided on the Cray Y-MP by the Pittsburgh Supercomputing Center. Discussions with Dr. R. Lavery and his suggestion of the use of the Hingerty et al. function to represent dielectric saturation effects are gratefully acknowledged. This project has benefited considerably from our participation in a series of CECAM Workshops in Paris on nucleic acid topics, organized by W. Olson, E. Westhof, and R. Lavery.

References and Notes

(1) Manning, G. S. *Quart Rev. Biophys.* **1978**, *11*, 179–246.
(2) Record, M. T., Jr.; Anderson, C. F.; Lohman, T. M. *Quart. Rev. Biophys.* **1978**, *11*, 103–178.
(3) Record, M. T., Jr.; Anderson, C. F.; Mills, P.; Mossing, M.; Roe, J.-H. *Adv. Biophys.* **1985**, *20*, 109–135.
(4) LeBret, M.; Zimm, B. H. *Biopolymers* **1984**, *23*, 271–285.
(5) Murthy, C. S.; Bacquet, R. J.; Rossky, P. J. *J. Phys. Chem.* **1985**, *89*, 701–710.
(6) Mills, P.; Anderson, C. F.; Record, M. T., Jr. *J. Phys. Chem.* **1985**, *89*, 3984–3994.
(7) Mills, P.; Paulsen, M. D.; Anderson, C. F.; Record, M. T., Jr. *Chem. Phys. Lett.* **1986**, *129*, 155–158.
(8) Mills, P.; Anderson, C. F.; Record, M. T., Jr. *J. Phys. Chem.* **1986**, *90*, 6541–6548.
(9) Paulsen, M. D.; Richey, B.; Anderson, C. F.; Record, M. T., Jr. *Chem. Phys. Lett.* **1987**, *139*, 448–452.
(10) Paulsen, M. D.; Richey, B.; Anderson, C. F.; Record, M. T., Jr. *Chem. Phys. Lett.* **1988**, *143*, 115–116.
(11) Conrad, J.; Troll, M.; Zimm, B. H. *Biopolymers* **1988**, *27*, 1711–1732.

(12) Valleau, J. P. *Chem. Phys.* **1989**, *129*, 163–175.
(13) Subramanian, P. S.; Ravishanker, G.; Beveridge, D. L. *Proc. Natl. Acad. Sci. U.S.A. 1988*, *85*, 1836–1840.
(14) Subramanian, P. S.; Beveridge, D. L. *J. Biomol. Struct. Dyn.* **1989**, *6*, 1093–1122.
(15) Westhof, E.; Beveridge, D. L. In *Water Science Reviews, The Molecules of Life*; Franks, F., Ed.; Cambridge University Press: New York, 1989; Vol. 5.
(16) Oosawa, F. *Polyelectrolytes*; Dekker: New York, 1971.
(17) Manning, G. S. *J. Chem. Phys.* **1969**, *51*, 924–933.
(18) Manning, G. S. *J. Chem. Phys.* **1969**, *51*, 934–938.
(19) Manning, G. S. *J. Chem. Phys.* **1969**, *51*, 3249–3252.
(20) Manning, G. S. *Annu. Rev. Phys. Chem.* **1972**, *23*, 117–140.
(21) Manning, G. S. *Biophys. Chem.* **1977**, *7*, 95–102.
(22) Manning, G. S. *Biophys. Chem.* **1978**, *9*, 65–70.
(23) Manning, G. S. *Acc. Chem. Res.* **1979**, *12*, 443–449.
(24) Fixman, M. *J. Chem. Phys.* **1979**, *70*, 4995–5005.
(25) Gueron, M.; Weisbuch, G. *Biopolymers* **1980**, *19*, 353–382.
(26) Klein, B. K.; Anderson, C. F.; Record, M. T., Jr. *Biopolymers* **1981**, *20*, 2263–2280.
(27) Anderson, C. F.; Record, M. T., Jr. *Annu. Rev. Phys. Chem.* **1982**, *33*, 191–222.
(28) Zimm, B. H.; LeBret, M. *J. Biomol. Struct. Dyn.* **1983**, *1*, 461–471.
(29) Anderson, C. F.; Record, M. T., Jr. In *Structure and Dynamics: Nucleic Acids and Proteins*; Clementi, E., Sarma, R. H., Eds.; Adenine Press: Albany, NY; 1983; pp 301–318.
(30) LeBret, M. Zimm, B. H. *Biopolymers* **1984**, *23*, 287–312.
(31) Bacquet, R.; Rossky, P. J. *J. Phy. Chem.* **1984**, *88*, 2660–2669.
(32) Klein, B. J.; Pack, G. R. *Biopolymers* **1983**, *22*, 2331–2352.
(33) Pack, G. R.; Klein, B. J. *Biopolymers* **1984**, *23*, 2801–2823.
(34) Pack, G. R.; Wong, L.; Prasad, C. V. *Nucleic Acids Res.* **1986**, *14*, 1479–1493.
(35) Matthew, J. B.; Richards, F. M. *Biopolymers* **1984**, *23*, 2743–2759.
(36) Wesnel, T. G.; Meares, C. F.; Vlachy, V.; Matthew, J. B. *Proc. Natl. Acad. Sci. U.S.A.* **1986**, *83*, 3267–3271.
(37) Troll, M. T.; Roitman, D.; Conrad, J.; Zimm, B. H. *Macromolecules* **1986**, *19*, 1186–1194.
(38) Jayaram, B.; Sharp, K.; Honig, B. *Biopolymers* **1989**, *28*, 975–993.
(39) Klapper, I.; Hagstrom, R.; Fine, R.; Sharp, K.; Honig, B. *Proteins* **1986**, *1*, 47–59.
(40) Gilson, M. K.; Sharp, K. A.; Honig, B. H. *J. Comput. Chem.* **1987**, *9*, 327–335.
(41) Hingerty, B. E.; Ritchie, R. H.; Ferrel, T. L.; Turner, J. E. *Biopolymers* **1985**, *24*, 427–439.
(42) Ramstein, J.; Lavery, R. *Proc. Natl. Acad. Sci. U.S.A.* **1988**, *85*, 7231–7235.
(43) Troll, M.; Zimm, B. H. *J. Phys. Chem.* **1983**, *87*, 3197–3201.
(44) Nordenskiold, L.; Chang, D. K.; Anderson, C. F.; Record, M. T., Jr. *Biochemistry* **1984**, *23*, 4309–4317.
(45) Forsen, S.; Drakenberg, T.; Wennerstro, H. *Quart. Rev. Biophys.* **1987**, *19*, 83–114.
(46) Anderson, C. F.; Record, M. T., Jr.; Hart, P. A. *Biophys. Chem.* **1978**, *7*, 301–316.
(47) Bleam, M. L.; Anderson, C. F.; Record, M. T., Jr. *Proc. Natl. Acad. Sci. U.S.A.* **1980**, *77*, 3085–3089.
(48) Bleam, M. L.; Anderson, C. F.; Record, M. T., Jr. *Biochemistry* **1983**, *22*, 5418–5425.
(49) Paulsen, M. D.; Anderson, C. F.; Record, M. T., Jr. *Biopolymers* **1988**, *27*, 1249–1265.
(50) Padmanabhan, B.; Richey, B.; Anderson, C. F.; Record, M. T., Jr. *Biochemistry* **1988**, *27*, 4367–4376.
(51) Reddy, M. R.; Rossky, P. J.; Murthy, C. S. *J. Phys. Chem.* **1987**, *91*, 4923–4933.
(52) Bacquet, R. J.; Rossky, P. J. *J. Phys. Chem.* **1988**, *92*, 3604–3612.
(53) Lee, W. K.; Gao, Y.; Prohofsky, E. W. *Biopolymers* **1984**, *23*, 257–270.
(54) Van Gunsteren, W. F.; Berendsen, H. J. C.; Guersten, R. C.; Zwinderman, H. R. *Ann. N.Y. Acad. Sci.* **1986**, *482*, 287.
(55) Swamy, K.; Clementi, E. *Biopolymers* **1987**, *26*, 1901–1927.
(56) Metropolis, N.; Rosenbluth, A. W.; Rosenbluth, M. N.; Teller, A. H.; Teller, E. *J. Chem. Phys.* **1953**, *21*, 1087–1092.
(57) Booth, F. *J. Chem. Phys.* **1950**, *19*, 391, 1327, 1615.
(58) Jayaram, B.; Fine, R.; Sharp, K.; Honig, B. *J. Phys. Chem.* **1989**, *93*, 4320–4327.
(59) Arnott, S.; Hukins, D. W. L. *Biochem. Biophys. Res. Commun.* **1972**, *47*, 1504–1510.
(60) Hansen, J. P.; McDonald, I. R. *Theory of Simple Liquids*; Academic Press: New York, 1976.
(61) Kalos, M. H.; Whitlock, P. A. *Monte Carlo Methods*; John Wiley & Sons: New York, 1986; Vol. 1.
(62) Ceperly, D.; Chester, G. V.; Kalos, M. H.; Phys. *Rev. B* **1977**, *16*, 3081–3099.
(63) Mezei, M. *J. Comput. Phys.* **1981**, *9*, 128–136.
(64) Beveridge, D. L.; et al. In Monte Carlo Computer Simulation Studies of the Equilibrium Properties and Structure of Liquid Water. *Molecular-Based Study of Fluids*; Haile, J. M., Mansoori, G. A., Eds.; American Chemical Society: Washington, DC, 1983; pp 297–351.
(65) Sharp, K.; Honig, B., unpublished results.
(66) Mezei, M.; Beveridge, D. L. *Free Energy Simulations in Computer Simulations and Biomolecular Systems*; Beveridge, D. L., Jorgensen, W. L., Eds.; New York Academy of Sciences: New York, 1986; Vol. 494 and references therein.
(67) Brunger, A.; Brooks, C. L.; Karplus, M. *Chem. Phys. Lett.* **1984**, *105*, 495–500.